

# Hygroscopicity of the submicrometer aerosol at the high-alpine site Jungfraujoch, 3580 m a.s.l., Switzerland

S. Sjogren<sup>1</sup>, M. Gysel<sup>1</sup>, E. Weingartner<sup>1</sup>, M. R. Alfarra<sup>1</sup>, J. Duplissy<sup>1</sup>, J. Cozic<sup>1</sup>, J. Crosier<sup>2</sup>, H. Coe<sup>2</sup>, and U. Baltensperger<sup>1</sup>

<sup>1</sup>Laboratory of Atmospheric Chemistry, Paul Scherrer Institut, 5232 Villigen, Switzerland

<sup>2</sup>School of Earth, Atmospheric and Environmental Science, University of Manchester, Manchester, UK

Received: 16 August 2007 – Published in Atmos. Chem. Phys. Discuss.: 19 September 2007

Revised: 7 July 2008 – Accepted: 21 July 2008 – Published: 30 September 2008

**Abstract.** Data from measurements of hygroscopic growth of submicrometer aerosol with a hygroscopicity tandem differential mobility analyzer (HTDMA) during four campaigns at the high alpine research station Jungfraujoch, Switzerland, are presented. The campaigns took place during the years 2000, 2002, 2004 and 2005, each lasting approximately one month. Hygroscopic growth factors ( $GF$ , i.e. the relative change in particle diameter from dry diameter,  $D_0$ , to diameter measured at higher relative humidity, RH) are presented for three distinct air mass types, namely for: 1) free tropospheric winter conditions, 2) planetary boundary layer influenced air masses (during a summer period) and 3) Saharan dust events (SDE). The  $GF$  values at 85% RH ( $D_0=100$  nm) were  $1.40\pm 0.11$  and  $1.29\pm 0.08$  for the first two situations while for SDE a bimodal  $GF$  distribution was often found. No phase changes were observed when the RH was varied between 10–90%, and the continuous water uptake could be well described with a single-parameter empirical model. The frequency distributions of the average hygroscopic growth factors and the width of the retrieved growth factor distributions (indicating whether the aerosol is internally or externally mixed) are presented, which can be used for modeling purposes.

Measurements of size resolved chemical composition were performed with an aerosol mass spectrometer in parallel to the  $GF$  measurements. This made it possible to estimate the apparent ensemble mean  $GF$  of the organics ( $GF_{org}$ ) using inverse ZSR (Zdanovskii-Stokes-Robinson) modeling.  $GF_{org}$  was found to be  $\sim 1.20$  at  $a_w=0.85$ , which is at the upper end of previous laboratory and field data though still in agreement with the highly aged and oxidized nature of the Jungfraujoch aerosol.

## 1 Introduction

Aerosol particles in the atmosphere affect the earth's radiation balance in various ways (e.g. Solomon et al., 2007). Firstly, aerosol particles absorb and scatter radiation. This direct aerosol effect is influenced by the hygroscopicity of the aerosol particles, which is determined mainly by their chemical composition. Secondly, the tendency for cloud formation and resulting cloud properties similarly depend on chemical composition as well as on size distribution of the aerosol particles (e.g. McFiggans et al., 2006). Thus the cloud albedo and the radiative properties of cloud droplets are influenced; this is termed the indirect aerosol effect. The presence of particulate water allows for physical processes (e.g., shape modification) or heterogeneous chemical reactions, which in turn influences the chemical composition. These processes are commonly referred to as the aging of aerosols.

Aerosols and their properties, such as hygroscopicity, are currently modeled in global climate models (GCMs), mostly to better predict the scattering properties and size distribution under varying humidity conditions (Randall et al., 2007). Relatively few measurements of background aerosol from the lower free troposphere exist (e.g. Kandler and Schütz, 2007; Swietlicki et al., 2008). To increase available data and validation possibilities four measurement campaigns at the high alpine site Jungfraujoch (JFJ), with a duration of about one month each, are presented here. During 2000, 2002, 2004 and 2005 the CLACE (CLOUD and Aerosol Characterization Experiment) field studies were performed within international collaborations, including both summer and winter seasons. The general goals of the field campaigns were i) a physical, chemical, and optical characterization of the aerosol at the JFJ in order to better quantify the direct aerosol effect, and ii) an investigation of the interaction of aerosol with clouds, for a better quantification of the indirect effect. The cloud forming processes were studied under



Correspondence to: E. Weingartner  
(ernest.weingartner@psi.ch)

different meteorological conditions, with a special focus on aerosol-cloud partitioning in mixed-phase clouds (Cozic et al., 2007; Verheggen et al., 2007). Further topics were the physical and chemical characterization of ice nuclei (Cozic et al., 2008b; Mertes et al., 2007), and the processes responsible for the formation of new particles in the free troposphere. Instrumentation was deployed to characterize the aerosol size distribution (scanning particle mobility sizer and optical particle counter), size segregated chemical composition (Aerodyne aerosol mass spectrometer, AMS) and hygroscopicity (hygroscopicity tandem differential mobility analyzer, HTDMA). In this study AMS and HTDMA results will be analyzed in greater detail.

Atmospheric aerosol components can be classified into inorganic and organic fractions (e.g. Kanakidou et al., 2005). The hygroscopic properties of most inorganic salts present in the atmospheric aerosol are known. Of the many organic species identified in the aerosol (e.g. Putaud et al., 2004), the hygroscopic properties of quite a few substances have been investigated. Inorganic salts (for instance ammonium sulfate,  $(\text{NH}_4)_2\text{SO}_4$ , and sodium chloride, NaCl, can show a hysteresis behavior during uptake and loss of water, i.e. by exhibiting a difference between the deliquescence and efflorescence relative humidities (DRH/ERH), and with a higher water content of the deliquesced than the effloresced particles in this relative humidity (RH) range. Conversely, organic constituents of the aerosol often do not show efflorescence which can contribute to an uptake of water at lower RH than the DRH of inorganic salts.

A method for characterizing water uptake of aerosol particles is the HTDMA (Liu et al., 1978; Rader and McMurry, 1986; Weingartner et al., 2002). The set-up used in three of the campaigns was a low-temperature HTDMA ( $-10^\circ\text{C}$  during the winter campaigns and  $0.5^\circ\text{C}$  during the summer campaign), and in the winter campaign 2005 measurements were done at laboratory temperature ( $25\text{--}33^\circ\text{C}$ ). Furthermore, measurements with an AMS supplied time- and mass-resolved chemical composition of sulfate, nitrate, ammonium and organics during the campaigns 2002, 2004 and 2005. The hygroscopic growth was predicted with the Zdanovskii-Stokes-Robinson (ZSR) relation using the measured composition from the AMS (Gysel et al., 2007; Stokes and Robinson, 1966), and compared with the hygroscopicity measured by the HTDMA.

## 2 Methods

### 2.1 Site and air mass types

The JFJ is a European high-alpine background site located on an exposed mountain col in the Bernese Alps, Switzerland, at 3580 m altitude ( $46.33^\circ\text{N}$ ,  $7.59^\circ\text{E}$ ). Throughout the year the station is within clouds about one third of the time (Baltensperger et al., 1998). During winter it is predominantly

in lower free tropospheric air masses. During summer the aerosol sampled is influenced by injections of air from the planetary boundary layer (PBL) (Baltensperger et al., 1997; Nyeki et al., 2000). The station is surrounded by glaciers and rocks, and no local vegetation is present. The JFJ boasts the highest European (electrical) railway station and is easily accessible throughout the year. Within the World Meteorological Organization (WMO) Global Atmosphere Watch (GAW) program continuous measurements of aerosol parameters have been performed at the JFJ site since 1995 (Collaud Coen et al., 2007). The research station is also part of the Swiss National Monitoring Network for Air Pollution (NABEL) and the Swiss Meteorological Institute (SMI).

The aerosol at the JFJ shows an annual cycle with highest mass concentrations in August to July and minimum concentrations in January to February, furthermore, the organic fraction increases during summer season (e.g. Cozic et al., 2008a; Nyeki et al., 1998; Weingartner et al., 1999). These are the major factors influencing the hygroscopic properties studied in this article. Based on comparison with the continuous aerosol measurements that are available for the JFJ since 1995, campaigns in 2000 and 2004 appear as typical winter conditions (with low aerosol concentration present in the free troposphere), while the campaign in 2002 is typical of summer conditions, and the 2005 campaign can be considered as spring-like conditions, with features situated in between winter and summer. In the following, the data are separated accordingly to these cases: non-disturbed lower free tropospheric winter conditions (abbreviated FT) and PBL influenced summer conditions (abbreviated PBL INF). Further, at times the JFJ is influenced by Saharan dust events (SDE). These events were detected according to the method described by Collaud Coen et al. (2004), which shows that during SDE the Angström exponent of the single scattering albedo (SSA) is negative. This method was also corroborated by size resolved chemical analysis by ion chromatography, where, during dust events,  $\sim 6\%$  of the total calcium concentration was found in the  $\text{PM}_{10}$  samples. Thus, a third type of air mass (abbreviated SDE) is distinguished here. The criterion used to identify SDE was an Angström exponent of the SSA less than  $-0.1$  for more than three hours. Conversely non-disturbed FT air masses were defined as the periods where the Angström exponent of the SSA was positive, and furthermore 1 h around each SDE was removed from the data to avoid transition periods.

### 2.2 Measurements

Several different inlets were used during the experiments. During three campaigns an interstitial inlet was operated with a  $\text{PM}_{10}$  or  $\text{PM}_{2.5}$  cyclone and sampled only the interstitial submicron-sized aerosol, with hydro-meteors being precipitated in the cyclone. A heated total inlet ( $25^\circ\text{C}$ ) was used during the last campaign, which was designed to evaporate the condensed water from cloud hydro-meteors thus

**Table 1.** Overview of the campaigns.

		Dry diameter, $D_0$ [nm]		
		50	100	250
<b>2000–Winter</b>				
Date	21.02 to 27.03.2000			
Number of scans* at RH=85%		1698	1855	1648
Number of humidograms		11	15	11
$T$ setting HTDMA, inlet type	$-10^\circ\text{C}$ , interstitial, $\text{PM}_1$			
<b>2002–Summer</b>				
Date	08.07 to 17.07.2002			
Number of scans* at RH=85%		528	746	517
Number of humidograms		4	43	4
$T$ setting HTDMA, inlet type	$0.5^\circ\text{C}$ , interstitial, $\text{PM}_1$			
<b>2004–Winter</b>				
Date	01.03 to 01.04.2004			
Number of scans* at RH=85%		499	1767	1295
Number of humidograms		4	4	4
$T$ setting HTDMA, inlet type	$-10^\circ\text{C}$ (as well as shortly $20^\circ\text{C}$ ), interstitial, $\text{PM}_{2.5}$			
<b>2005–Spring-like</b>				
Date	13.02 to 16.03.2005			
Number of scans* at RH=85%		306	1533	162
Number of humidograms		6	6	6
$T$ setting HTDMA, inlet type	$25^\circ\text{C}$ , total inlet			

\*Each scan had a duration of 300 s.

sampling the sum of all particles including both cloud droplet residual and interstitial particles. The total inlet has an upper 50% cut-off diameter of  $40\ \mu\text{m}$  at wind speeds up to  $20\ \text{ms}^{-1}$  according to calculations by Weingartner et al. (1999). The percentage of time during which wind speeds above  $20\ \text{ms}^{-1}$  were encountered at the site over the last 9 years was low: 2.6%. It is important to ensure that the actual cut-off is sufficiently large to sample cloud droplets efficiently and that the heating does not disturb the particle size distributions. Henning et al. (2002) showed by differentiating size distributions measured downstream of both total and interstitial inlets and comparison to cloud microphysical measurements (FSSP) that the total inlet has a sufficient sampling efficiency for cloud droplets under the given conditions and that the heating does not otherwise disturb the particle size distributions. The difference in response downstream of the two different inlets provides insight into the fractionation of aerosol particles between the cloud phase and the interstitial phase. Table 1 lists the dates for the campaigns as well as details of instruments used and setup of the HTDMA.

### 2.3 AMS (Aerosol Mass Spectrometer)

An Aerodyne quadrupole AMS (Jayne et al., 2000) was used to provide on-line, quantitative measurements of the total mass and size distributed non refractory chemical composition of the submicron ambient aerosol at a high temporal

resolution. The instrument works by sampling air through an aerodynamic lens to form a particle beam in a vacuum and accelerating the focused beam of particles as a function of their momentum towards a tungsten heater ( $550^\circ\text{C}$ ) that flash vaporizes the particles. The volatilization stage is performed adjacent to an electron impact ionizer (about  $70\ \text{eV}$ ) and the ions are analyzed by a quadrupole mass spectrometer (QMA 410, Balzers, Liechtenstein) with unit mass-to-charge ( $m/z$ ) resolution. In typical field operation, the AMS alternates between two modes: (i) in the mass-spectrum (MS) mode the averaged chemical composition of the non-refractory (NR) aerosol ensemble is determined by scanning the  $m/z$  spectrum with the quadrupole mass spectrometer, without size resolved information, (ii) using the aerosol time-of-flight (ToF) mode selected  $m/z$  representative of key chemical components can be resolved as a function of the vacuum aerodynamic diameter of the particles. More detailed descriptions of the AMS measurement principles and various calibrations (Canagaratna et al., 2007; Jayne et al., 2000), its modes of operation (Jimenez et al., 2003) and data processing and analysis (Allan et al., 2003; Allan et al., 2004) are available. The AMS supplies the concentrations of inorganic ions, i.e. sulfate, nitrate and ammonium. These ions account for 96% of the composition of inorganic ions at the JFJ (Cozic et al., 2008a; Henning et al., 2003; Krivacsy et al., 2001). Furthermore the total concentration of the organic content is

supplied, although no detailed speciation is possible. Mass loadings at the JFJ site are generally low. Therefore 3-h averages were calculated as a compromise between counting statistics and time resolution.

#### 2.4 Black carbon concentration

During the first two campaigns 2000 and 2002 the black carbon (BC) concentration was measured with an AE31 Aethalometer (wavelength  $\lambda=880$  nm was used) (Weingartner et al., 2003). During the last two campaigns BC was measured with a multiple angle absorption photometer (MAAP, at  $\lambda=630$  nm) as well as with an AE31 Aethalometer (at  $\lambda=880$  nm). A mass absorption efficiency of  $7.6\text{ m}^2\text{g}^{-1}$  for winter and  $11.1\text{ m}^2\text{g}^{-1}$  for summer was used for the MAAP data (Cozic et al., 2008a). BC concentrations from the aethalometer were determined accordingly, taking advantage of a high correlation between these two instruments during simultaneous measurements (Cozic et al., 2008a). As no size resolved BC measurements were available it was assumed that the BC fraction in each size range was independent of size and thus equal to the BC fraction in  $\text{PM}_{10}$  (defined as the sum of the AMS and the BC data). The choice of the mass absorption efficiency for the BC concentration and its size independence are not critical due to the low sensitivity of the hygroscopicity closure to these assumptions. The measured BC volume fraction during the CLACE campaigns was always less than 10%. Therefore even completely ignoring BC in the ZSR predictions increases predicted  $GF$ s less than 0.02, which is well within our stated uncertainty.

#### 2.5 HTDMA (Hygroscopicity Tandem Differential Mobility Analyzer)

Briefly, the HTDMA functions as follows: a differential mobility analyzer (DMA1) selects a monodisperse aerosol size cut with mobility diameter,  $D_0$ , under dry conditions. The aerosol then passes through a humidifier with a controlled higher RH, and the mobility diameter  $D$  is measured with a second DMA (DMA2). The two DMAs are similar to the TSI 3071 type. The relevant RH in DMA2 was determined by measurement of the system temperature and the DMA2 excess sheath air dew point using a dew point mirror (model 2002 Dewprime, EdgeTech). The accuracy of the RH measurement at RH=85% is  $\Delta\text{RH}=\pm 1.1\%$ , with temperature gradients  $<0.1\text{ K}$  in DMA2 and an accuracy of the measured temperature difference between dew point and DMA2 temperature of  $\pm 0.2\text{ K}$ . The residence time of the sampled aerosol at the set RH was  $\sim 20$  s before size measurement (Sjogren et al., 2007). The HTDMAs were employed in slightly different ways during the different campaigns (see Table 1). In general the HTDMA measured at a constant RH which was set to 85%. On occasions the RH-dependence of the hygroscopic growth was investigated by both increasing and decreasing the RH in DMA2 between 10 and 85%.

These are known as the dehydration and hydration modes of operation, respectively. This allows for detecting potential hysteresis effects in the hygroscopic growth behavior with distinct efflorescence and deliquescence transitions. The hydration mode, where the mono-modal dry particles were exposed to a monotonically increasing RH in the HTDMA prior to the size measurement in DMA2 (allowing measurements of DRH), was applied during all campaigns, and is also the mode of operation used during measurements at constant RH. The dehydration mode, where the dry particles are first exposed to  $\text{RH}>80\%$  using a pre-humidifier before monotonically lowering the RH towards the RH in DMA2 (Gysel et al., 2004; Sjogren et al., 2007), was mainly applied during the 2004 winter campaign (allowing measurements of ERH).

The hygroscopic growth factor ( $GF$ ) indicates the relative increase in mobility diameter of particles due to water absorption at a certain RH, and is defined as

$$GF(\text{RH}) = \frac{D(\text{RH})}{D_0} \quad (1)$$

where  $D(\text{RH})$  is the mobility diameter at a specific RH and  $D_0$  is the particle mobility diameter measured under dry conditions (91% of the data were with DMA1 at  $\text{RH}<15\%$ ). However to increase available data we included periods where the RH in DMA1 was up to 35%, where the  $GF$  is relatively low ( $<1.03$ ) for the ambient aerosol (see below).

Mobility diameter growth factors obtained with an HTDMA are only equal to volume equivalent growth factors if the particles do not change their shape during water uptake. This assumption is justified as the hygroscopicity was characterized by a continuous growth curve for the majority of the time (see below), thus the particles can be considered liquid and consequently roughly spherical at all measured RH.

During the first three campaigns both DMAs and the humidifier were inserted in a well-circulated water bath, ensuring constant temperature as indicated. The aerosol line was cooled and insulated from the outside of the building to the entry of the first DMA. This ensured that no artifacts during the sampling occurred (i.e. volatilization of semi-volatile material), as the measurements were performed close to ambient temperatures (Gysel et al., 2002; Weingartner et al., 2002). During the campaign in 2005 the first DMA was maintained at the laboratory temperature ( $25\text{--}33^\circ\text{C}$ ) and only DMA2 was kept at a constant temperature in a water bath ( $22.8^\circ\text{C}$ ) (Sjogren et al., 2007). This was done because of the functionality of the HTDMA used, and because it was deduced from the three first campaigns that temperature artifacts were negligible (i.e. compared to measurement uncertainties). The HTDMA data were averaged to 3 h, in order to match the AMS time series. The performance of the instruments was verified with extensive testing with  $(\text{NH}_4)_2\text{SO}_4$  and NaCl before the campaigns. During 2004 and 2005 these salts were also measured at the JFJ. The growth of  $(\text{NH}_4)_2\text{SO}_4$  and NaCl particles was compared with the theoretical prediction

using the Aerosol Diameter-Dependent Equilibrium Model (ADDEM) (Topping et al., 2005a, b), and corresponded to within less than 0.04 in  $GF$  at 85% RH.

### 2.5.1 Inversion algorithm

Atmospheric particles of a defined dry size typically exhibit different growth factors. This is due to either external mixing of particles in an air sample or variable relative fractions of different compounds in individual particles (the latter hereinafter referred to as quasi-internally mixed). A mono-modal growth distribution without spread can only be expected in very clean and homogeneous air parcels. For further details on mixing states see e.g. Buzorius et al. (2002). Growth factor probability density functions (GF-PDF,  $cGF$ ) are retrieved from each measurement, and normalized such that  $\int c(GF)dGF=1$ . The inversion method applied to the raw data (Gysel et al., 2008<sup>1</sup>) has been tested and applied to ambient HTDMA data previously (Gysel et al., 2007; Allan et al., 2008). This method uses a full TDMA transfer forward function in combination with a  $\chi^2$  minimization algorithm to retrieve the GF-PDF from the measured  $GF$  distribution. This approach is similar to the TDMAfit algorithm by Stolzenburg and McMurry (1988) with the difference that the GF-PDF is assumed to be a piecewise linear function with fixed support points instead of a superposition of multiple Gaussians. Using a piecewise linear function with fixed support points is similar to the inversion algorithm described by Cubison et al. (2005). Here a resolution of  $\Delta GF=0.15$  was chosen for the support points. The AMS provides chemical composition data for the bulk submicron aerosol in the air sample, whereas no information on the mixing state of the aerosol is obtained. GF-PDFs obtained with the HTDMA provide some information on the mixing state. The ensemble mean growth factor  $GF^*$  is defined as volume weighted (3<sup>rd</sup>-moment) mean growth factor of the GF-PDF:  $GF^*=(\int GF^3 c(GF) dGF)^{1/3}$ .  $GF^*$  represents the growth factor that would be observed if the absorbed water was equally distributed among all particles in a sample. Thus  $GF^*$  is the quantity to be compared with growth factor predictions based on bulk chemical composition data obtained by the AMS (see below), also for externally mixed aerosols. However, this is not the case if a significant mass fraction cannot be measured by the AMS because of large contributions of refractory material such as dust, black carbon or sea salt.

The standard deviation  $\sigma$  of the inverted GF-PDF is used as a measure for the spread of growth factors. The lower detection limit for spread of growth factors is  $\sigma=0.10$  with a resolution of  $\Delta GF=0.15$  as chosen here for the HTDMA data inversion. The spread obtained with pure ammonium

sulfate at 85% RH is  $\sigma<0.05$ , however, such small  $\sigma$  can only be detected when counting statistics allow for inversion with higher resolution. Therefore any  $\sigma \geq 0.15$  shows that the aerosol is externally mixed or quasi-internally mixed with substantial spread of growth factors, while any  $\sigma \leq 0.10$  indicates absence of distinct growth modes, i.e. an internal mixture or a quasi-internal mixture with limited spread of growth factors. We use the  $\sigma$  not only to describe the spread of a single mode, but also in the sense of describing a broader distribution, or describing cases which are clearly bimodal. Two HTDMA measurement examples (red) and corresponding inverted growth factor distributions (green) as well as the inverted growth distribution reprocessed through the HTDMA forward model (blue) are shown in Fig. 1. Panel (A) shows an aerosol ( $D_o=100$  nm) observed during undisturbed FT conditions with  $GF^*=1.28$  and  $\sigma=0.08$ , indicating that it was internally mixed. Panel (B) shows an aerosol observed during an SDE with  $\sigma=0.22$ . This aerosol is obviously externally mixed with two distinct modes at  $GF=1.05$  and  $GF=1.45$ , whereof the former can be attributed to mineral dust. The  $GF^*$  is 1.227 and is not representative of the hygroscopic behavior of the aerosol but would be the value to compare with the predicted hygroscopicity from the ensemble chemical composition, which would need to take mineral dust into account. In this case the blue line does not exactly follow the measurement because of the limited resolution of the inversion. However, better results cannot be obtained even with increasing the resolution, because the measurement uncertainties are too big at such a low number of measured counts.

### 2.5.2 Correction of HTDMA data to 85% RH

The measurements were generally done at 85% RH. To obtain a more complete time series data set, data between 80 and 90% RH were corrected to 85% RH using the following equation:

$$k(GF, a_w) = \frac{(GF^3 - 1)(1 - a_w)}{a_w} \quad (2)$$

$$\Leftrightarrow GF(a_w, k) = \left(1 + k \frac{a_w}{1 - a_w}\right)^{1/3}$$

where  $k$  captures all solute properties.  $a_w$  is the water activity. First the  $k$ -value was calculated from the measured  $GF$  and RH (first line of Eq. 2), and then the corresponding corrected  $GF$  at 85% was calculated using this  $k$  (second line of Eq. (2)). Equation (2) is equivalent to Eq. (4) in the paper by Gysel et al. (2004) with  $k=(M_w \rho_s i_s)/(\rho_w M_s)$ , where  $M_w$  is the molar mass and  $\rho_w$  the density of water, and  $M_s$  the molar mass,  $\rho_s$  the density and  $i_s$  the van't Hoff factor of the solute. Equation (2) is also equivalent to Eq. (1) in the paper by Dick et al. (2000) with  $a=k$  and  $b=c=0$ , where  $a$ ,  $b$ , and  $c$  are their model parameters. More details about the theoretical background of the functionality of Eq. (2) are given in

<sup>1</sup>Gysel, M., McFiggans, G. B., and Coe, H.: Inversion of Tandem Differential Mobility Analyser (TDMA) Measurements, J. Aerosol Sci., submitted, 2008.

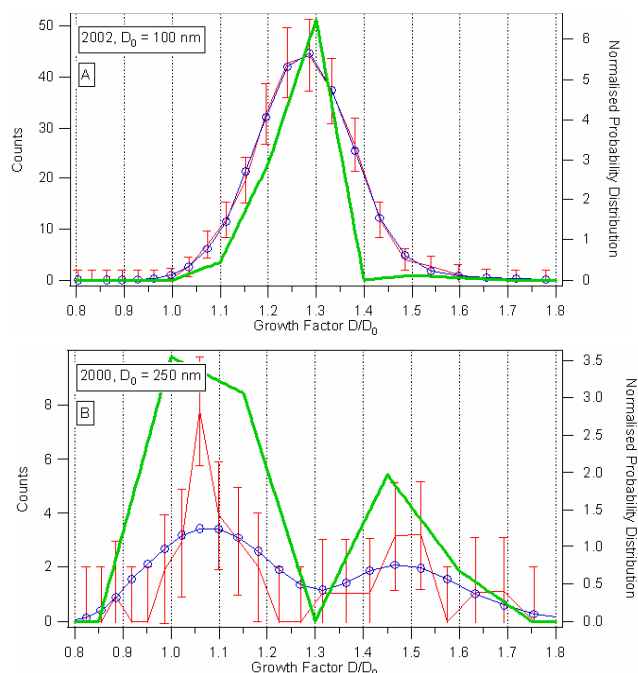


**Fig. 1.** Typical examples of growth factor distributions at RH=85% of  $D_0=100$  nm particles ( $GF=1.28$ ) and  $\sigma=0.08$  (Panel (A), 12 July 2002 18:00) and of  $D_0=250$  nm particles during a SDE (Panel (B), 17 March 2000 20:24), with a first mode at  $GF=1.05$  and a second mode at  $GF=1.45$  (overall  $\sigma=0.22$ ). The red line and points (left axis) refer to measured particle counts, the green line is the inverted  $GF$  distribution (right axis) and the blue line inverted growth distribution reprocessed through the forward model (left axis). Error bars indicate the estimated counting uncertainty of the measurement.

Kreidenweis et al. (2005). Using a constant  $k$ -value for RH corrections is equivalent to a constant van't Hoff factor. This assumption is justified for differences of  $\pm 5\%$  RH as chosen here.

## 2.6 Prediction of hygroscopic growth factors

Prediction of hygroscopic growth factors with Köhler theory requires detailed knowledge of particle composition as well as a thermodynamic model, which describes the concentration dependence of the water activity for such a mixture. The hygroscopic growth factor of a mixture,  $GF_{\text{mixed}}$ , can be estimated from the growth factors of the individual components of the aerosol and their respective volume fractions,  $\varepsilon$ , with the ZSR relation (Stokes et al., 1966):

$$GF_{\text{mixed}} = \left( \sum_k \varepsilon_k GF_k^3 \right)^{1/3} \quad (3)$$

where the summation is performed over all compounds present in the particles. Solute-solute interactions are neglected in this model and volume additivity is also assumed.

**Table 2.** Hygroscopic growth factors for pure substances and physical properties used (Bulk properties, Topping et al., 2005a).

Substance	$GF$ (at $a_w = 0.85$ )	Density [ $\text{kg m}^{-3}$ ]
$(\text{NH}_4)_2\text{SO}_4$	1.56	1769
$\text{NH}_4\text{HSO}_4$	1.62	1780
$\text{NH}_4\text{NO}_3$	1.59	1720
$\text{H}_2\text{SO}_4$	1.88	1830
BC	1.0	2000
Organics	1.20 <sup>a</sup>	1400 <sup>b</sup>

<sup>a</sup> The growth factor of the organics was chosen to give a best fit between measurement and model. See Section 3.1 for discussion of this value.

<sup>b</sup> The density of organics was chosen to represent oxidized organics in aged atmospheric aerosol (Alfarra et al., 2006; Dinar et al., 2006).

The AMS measured size-resolved mass concentrations of ammonium ( $\text{NH}_4^+$ ), sulfate ( $\text{SO}_4^{2-}$ ), nitrate ( $\text{NO}_3^-$ ), and organics with high temporal resolution during the last three campaigns: 2002, 2004 and 2005. The  $\text{PM}_{10}$  aerosol at the JFJ was mostly neutralized with ammonium (Cozic et al., 2008a), according to AMS data and  $\text{PM}_{10}$  filter samples. The pairing of the inorganic ions, which is required for the ZSR relation, is unambiguous for aerosols neutralized by a single cation. However, occasionally the measured ammonium concentration was insufficient to fully neutralize the sulfate, thus indicating an acidic aerosol. In such cases the ion-pairing becomes ambiguous and therefore an adequate ion-pairing scheme must be applied. We used the simplified ion-pairing scheme presented by Gysel et al. (2007), which has a direct analytical solution and deviations of corresponding ZSR predictions from full thermodynamic models are minuscule for the relevant inorganic mixtures. Growth factors of pure inorganic salts are obtained from ADDEM (Topping et al., 2005a, b; see Table 2). Densities used to convert mass fractions measured by the AMS into volume fractions required for the ZSR relation (Eq. 3) are also provided in Table 2.

The AMS composition data were integrated over a narrow size range from 88–196 nm vacuum aerodynamic diameter ( $d_{va}$ ), which corresponds to a volume weighted mean mobility diameter of  $d_{\text{mob}}=100$  nm (49–122 nm). The chosen width of the size range is a compromise between size resolution and signal statistics. Conversion of vacuum aerodynamic diameters into mobility diameters was done according to the equations provided in Zelenyuk et al. (2006), assuming a dynamic shape factor of one and using a particles density of  $1565 \text{ kg/m}^3$ , as calculated from the campaign average composition.

The growth factor of the organic aerosol fraction, the only remaining unknown variable in the ZSR equation (Eq. 3), cannot be calculated based on the chemical information

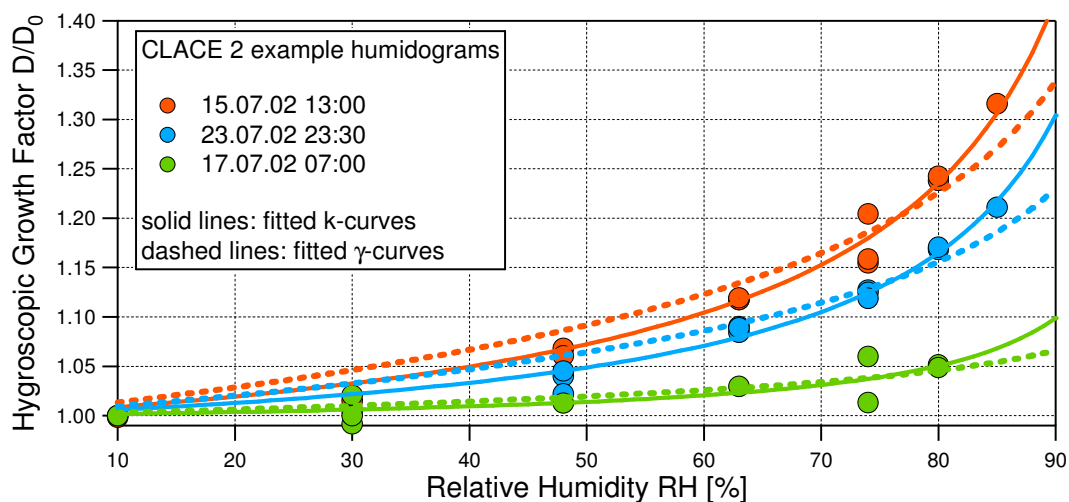


**Fig. 2.** Typical humidograms of particles with  $D_0=100$  nm sized particles during July 2002 (the other campaigns gave similar results). The hygroscopicity at the JFJ varies with varying season and origin of air parcels, but the water uptake at a specific time can be well described as a function of RH with a single-parameter model (solid lines).

obtained with the AMS. Therefore the ZSR model could be used to infer the apparent ensemble mean growth factor of the organics,  $GF_{\text{org}}$ , as detailed in Sect. 3.2.

### 3 Results

#### 3.1 Hygroscopicity at the JFJ

The RH-dependence of  $GF$  was measured by variation of the RH in the HTDMA between 10 and 85%. Figure 2 shows three examples of typical humidograms showing the features observed at the JFJ. Generally a continuous growth without differences between hydration and dehydration operating mode was found, thus indicating absence of phase changes. This does not exclude existence of efflorescence at  $RH < 10\%$ , because our measurements were technically limited to  $RH > \sim 10\%$ . Such continuous growth is expected and has been reported for complex mixtures with an increasing number of organic components (Marcolli et al., 2004; Marcolli and Krieger, 2006). The aerosol at the JFJ seems to exist predominantly as dissolved liquid or amorphous particles. Furthermore, the growth curves can be well described with the single-parameter ( $k$ ) semi-empirical model given in Eq. (2), as can be seen from the solid lines in Fig. 2. The growth curves were also fitted with an empirical power law fit  $GF=(1-a_w)^\gamma$  (Swietlicki et al., 2000), dashed lines in Fig. 2, but for this model we found consistently larger  $\chi^2$ -residuals than with the former model. As can be seen from Figs. 2, 3 and 4 the magnitude of the hygroscopic growth at the JFJ varies substantially over time, but the RH-dependence at any time can be captured with a single parameter ( $k$ ).

Figure 3 shows the temporal evolution of  $GF$  distributions for a period of the campaign in 2000. Several SDE were observed, as indicated with the shaded areas in Panel (A). During undisturbed FT conditions, a size dependence of the growth factor can be seen, with larger growth for larger particles. This feature, which has previously been shown by Weingartner et al. (2002), was also observed during the other campaigns and is attributed to a size dependent chemical composition. This is confirmed by larger  $k$ -values at larger dry diameters (top panel of Fig. 3), which are a measure of the hygroscopicity without the influence of the Kelvin effect. The ensemble  $k$ -values have been calculated from the ensemble mean growth factor  $GF^*$  using Eq. (2), whereas the water activity corresponding to the measured RH has been calculated assuming a surface tension of pure water. The size dependence of the hygroscopicity can most likely be attributed to an increasing fraction of organic compounds with decreasing dry diameter, as observed with AMS measurements during the summer 2002 campaign (Alfarra, 2004). During major SDE two distinct growth modes can be seen for the 250 nm particles, while no clear change in hygroscopic behavior is seen for the 50 nm particles. This is also reflected in strongly decreasing  $k$ -values at  $D_0=250$  nm, while little or no changes occur at  $D_0=100$  and 50 nm. Thus mineral dust particles are only found at larger sizes. As during SDE larger sized particles are more externally mixed, the reduction of the  $k$ -value in these periods only reflects the influence of the increasing amount of particles, presumably mineral dust, with lower hygroscopicity, not the  $k$ -value of each mode. Some externally mixed particles with lower hygroscopicity can also be found when the site is not influenced by a pronounced SDE event (e.g. Fig. 3,  $D_0=250$  nm, 13.03.–15.03.00). However, such external mixing is much

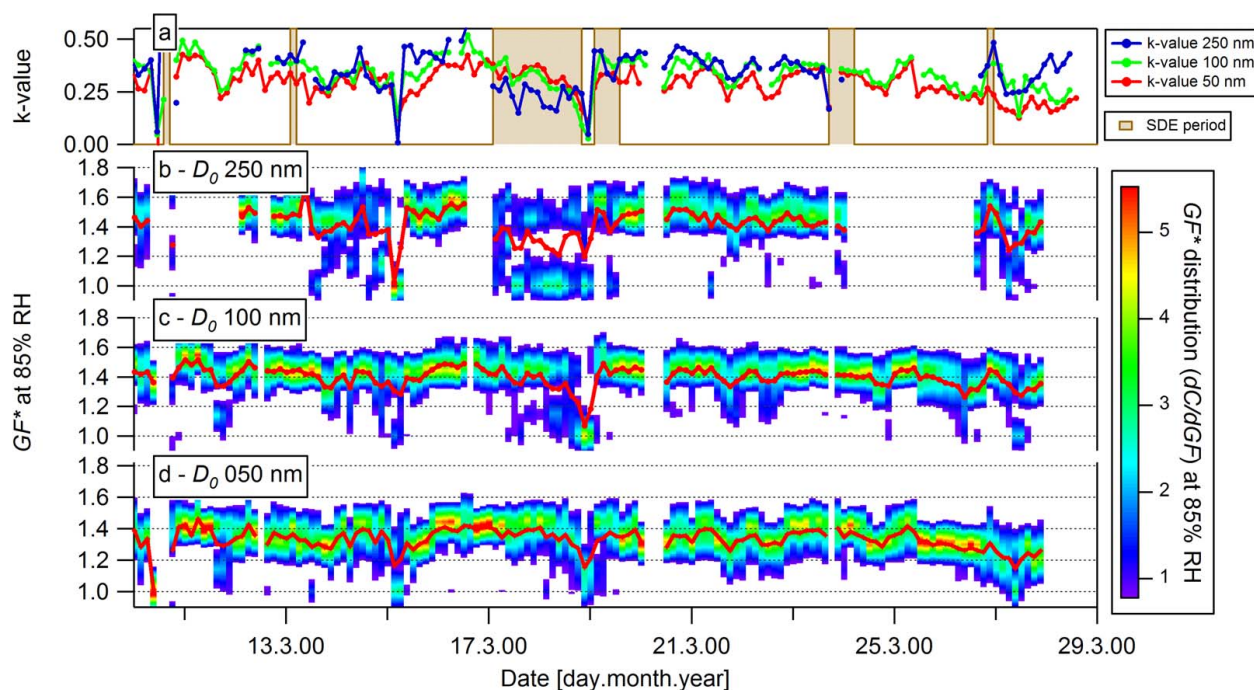


**Fig. 3.** Temporal evolution of  $GF$  distributions for  $GF$  all measured sizes ( $D_0=50, 100, 250$  nm) at  $RH=85\%$ , during year 2000. Panel (a) shows the  $k$ -values indicating the hygroscopicity of the aerosol. The red lines on panels (b), (c) and (d) represent the ensemble mean growth factor  $GF^*$ .

**Table 3.** Summary of mean  $GF^*$ , median  $GF^*$  and mean spread  $\sigma$  of the  $GF$  distributions for the campaigns.

Campaign date	Feb–Mar 2000			Jul 2002			Mar 2004			Feb–Mar 2005		
Season	Winter			Summer			Winter			Spring-like		
Dry diameter $D_0$ [nm]	50	100	250	50	100	250	50	100	250	50	100	250
Mean $GF^*$ at 85% RH	1.33	1.40	1.41	1.26	1.29	1.35	1.34	1.40	1.47	1.30	1.35	1.42
–Std.dev. of $GF^*$	0.091	0.104	0.133	0.090	0.076	0.081	0.122	0.112	0.114	0.081	0.076	0.076
Number of scans	1698	1855	851	528	746	517	499	1767	1295	306	1533	162
Mean spread $\sigma$	0.13	0.15	0.19	0.08	0.10	0.12	0.11	0.13	0.15	0.17	0.16	0.16
–Std.dev. of $\sigma$	0.041	0.046	0.070	0.045	0.043	0.043	0.050	0.055	0.063	0.095	0.058	0.089
Median $GF^*$ at 85% RH	1.34	1.41	1.44	1.25	1.29	1.36	1.33	1.41	1.48	1.31	1.34	1.41

less frequent and less pronounced than during SDE events, as discussed below with the overall statistics.

In summer, a strong diurnal variation is typically found in most aerosol variables (Lugauer et al., 2000). During the 2002 campaign this diurnal variation was also present in the observed mass loadings, though to a slightly lesser extent (Alfarra, 2004). However, the mass fractions of different components did not vary to a large degree during this diurnal variation, resulting in a fairly constant hygroscopicity on a timescale of hours seen both in the HTDMA results and in the closure (Fig. 4). However, more data with days showing a strong diurnal variation are required for a conclusive description of this influence. As can be seen from the mean  $GF^*$  values in Table 3, the summer campaign is characterized by lower hygroscopicity, due to a higher organic loading (68% in summer compared to 42% in winter). This is most proba-

bly due to higher emission rates of secondary organic aerosol (SOA) precursors and higher photo-oxidation activity, which can also be transported upwards through valley venting.

### 3.2 Apparent growth factor of the organics

The growth factor of the organic aerosol fraction cannot be calculated from the AMS data, because neither a detailed speciation nor a characterization in terms of functional groups and molecule sizes is available. Therefore the apparent ensemble mean growth factor of the organics,  $GF_{org}$ , was determined with an inverse modelling approach:  $GF_{org}$  was fitted such that best possible agreement between measured growth factors and corresponding ZSR predictions was achieved. We name it “apparent  $GF_{org}$ ” because it may well be different from the ensemble mean growth factor of the

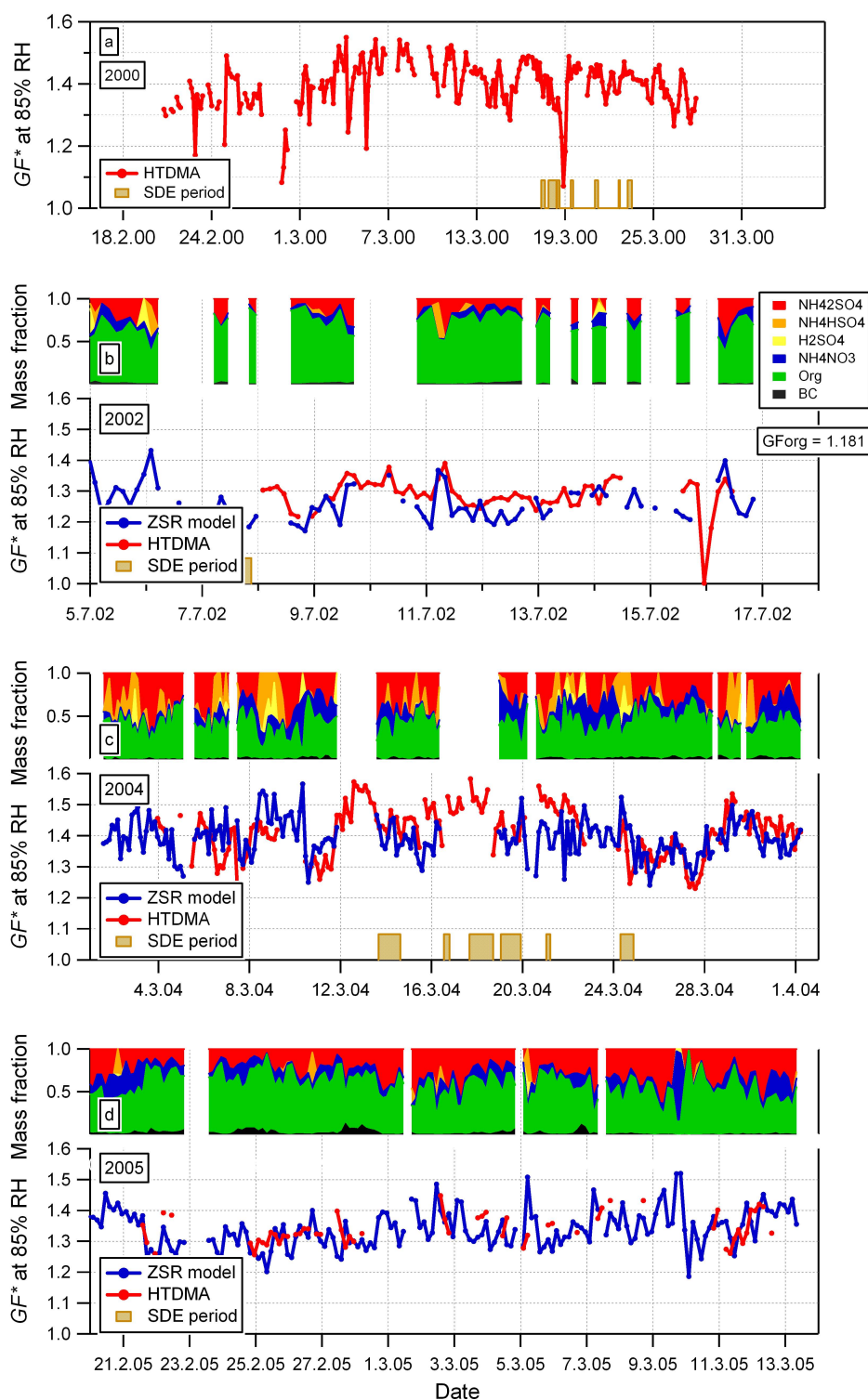


**Fig. 4.** Time series of the  $GF^*$  at RH=85% for  $D_0=100$  nm particles at the JFJ for each campaign measured (each lower panel), as well as the chemical composition (each top panel). The predicted  $GF^*$  from composition data is shown as the blue line in the  $GF$  panels and the measured in red. During winter 2000 no high time resolution composition data were available.

organics in pure form. For example positive/negative interactions between the organic and inorganic solutes in the mixed solution would result in an enhanced/reduced apparent  $GF_{\text{org}}$  compared to the growth of the organics in pure form. A constant (time independent)  $GF_{\text{org}}$  can either be fitted such that the sum of all residuals between each pair of measured and predicted  $GF^*$  is minimised, or alternatively such that the correlation between all measured and predicted  $GF^*$  has a unit slope. These two approaches deliver equivalent results with less than two percent difference in fitted  $GF_{\text{org}}$ . The latter alternative is presented in the following because it simplifies the discussion and sensitivity analysis of the results.

Figure 4 shows a time series of the volume weighted ensemble mean growth factor,  $GF^*$ , measured by the HTDMA for  $D_0=100$  nm particles along with the corresponding ZSR predictions using the best fit apparent  $GF_{\text{org}}$ , which was found to be  $\sim 1.2$  at  $a_w=0.85$  for the campaigns 2002, 2004 and 2005 (no high time resolution composition data were available for 2000). Note, this value of  $GF_{\text{org}}$  corresponds to a growth factor of  $\sim 1.18$  for 100 nm particles at RH=85% due to the influence of the Kelvin effect. Correlation coefficients of  $r\approx 0.35\text{--}0.60$  are achieved for the three campaigns with the above constant  $GF_{\text{org}}$ . This seems rather low, however, the actual variability of  $GF^*$  is small compared to the measurement uncertainties imposed by statistical noise in both HTDMA and AMS data due to very low aerosol loadings at the Jungfraujoch, thus explaining relatively low correlation coefficients. For the same reason no sensible results can be achieved by fitting a time dependent  $GF_{\text{org}}$  and hence it is not possible to extract temporal trends of the apparent  $GF_{\text{org}}$ . Reduction of the apparent  $GF_{\text{org}}$  to 1.15, 1.10 and 1.00 at  $a_w=0.85$  decreases the slope of the correlations to  $\sim 0.93$ ,  $\sim 0.86$  and  $\sim 0.75$ , respectively, indicating that the apparent  $GF_{\text{org}}$  is likely to be  $\geq 1.15$  and most likely  $> 1.10$ .

An apparent  $GF_{\text{org}}$  in the order of 1.2 at  $a_w=0.85$  is at the upper end of the range reported in laboratory experiments for SOA (e.g. Varutbangkul et al., 2006; Baltensperger et al., 2005) or humic-like substances (HULIS) extracted from ambient samples (e.g. Gysel et al., 2004). However, Duplissy et al. (2008) have shown that the  $GF$  of SOA measured in smogchamber experiments can be substantially higher when using lower, atmospherically relevant precursor concentrations. Furthermore the SOA  $GF$  increases continuously with ongoing photochemical reaction and can reach  $\sim 1.2$  at  $a_w=0.85$  for  $\alpha$ -pinene SOA. Ensemble  $GF$ s derived for the organic aerosol fraction in previous ambient hygroscopicity closure studies looking at SOA dominated or aged air masses are slightly smaller (Aklilu et al., 2006; Gysel et al., 2007) or comparable (Carrico et al., 2005) to the findings in this study. The air masses at the JFJ are representative of an aged aerosol and therefore a relatively high ensemble organic  $GF$  can be expected. This is corroborated by the fact that the mass spectra obtained by the AMS at the Jungfraujoch are characterized by the absence of the hydrocarbon mass fragments pattern from the ion series  $C_n H_{2n+1}^+$  (i.e.  $m/z$  43, 57,

71, 85), indicating that little unprocessed primary organic material is present (Zhang et al., 2005; Alfarra et al., 2006). On the other hand, the spectra are dominated by mass fragment  $m/z$  44 which arises from  $\text{CO}_2^+$  as a result of the thermal decomposition of highly oxygenated organic compounds in the AMS. This mass spectral pattern is typical for processed and aged organic aerosol (Alfarra et al., 2006; Zhang et al., 2007). These findings indicate on the one hand that the apparent  $GF_{\text{org}}$  tends to increase from polluted towards remote locations, and on the other hand that it is unlikely to reach values significantly higher than  $GF_{\text{org}}\approx 1.2$  at  $a_w=0.85$  as estimated for the Jungfraujoch.

During SDE there will be an increased fraction of mostly insoluble mineral dust material (Vlasenko et al., 2006) which is not detected in the AMS. This will lead to an increase in the predicted  $GF$  compared to the measured one. However, during 2004 some SDE were detected when both instruments were in operation, but the residuals from measured minus predicted hygroscopicity for these SDE were similar to FT conditions. Probably the mass fraction of mineral dust components were not sufficiently high at sizes  $< 250$  nm to significantly influence the ensemble mean growth factor  $GF^*$ .

Recently, Aklilu et al. (2006) and Gysel et al. (2007) have found significant discrepancies between measured and predicted  $GF$ s if substantial mass fractions of ammonium nitrate were present. Aklilu et al. (2006) speculated that the ZSR relation may not hold in the presence of ammonium nitrate, whereas Gysel et al. (2007) concluded that the most likely cause for the discrepancies in their case was an evaporation artifact of ammonium nitrate in the HTDMA, which was operated at  $\sim 25^\circ\text{C}$  and with a residence time of  $\sim 60$  s. No systematic prediction bias for data points with high ammonium nitrate mass fraction was found in the data set presented here, indicating that no evaporation artifacts occurred. An important difference is that the HTDMA measurements of this study were mostly done at low temperatures ( $T=-10$  to  $0.5^\circ\text{C}$ ) and the residence time was kept short ( $\sim 20$  s), thus minimizing potential evaporation artifacts.

### 3.3 Frequency distributions of $GF^*$ and $\sigma$

Panels (A), (D) and (G) of Fig. 5 show the averages of the normalized measured  $GF$  distributions for each dry size studied and for each air mass category. The air mass types distinguished in this analysis are the SDE, the non-disturbed FT conditions as well as the cases influenced by injections from planetary boundary layer air (i.e., during summer, PBL INF). These averaged growth distributions illustrate the mean number fraction of particles in a defined air mass type exhibiting a certain growth factor, unlike Fig. 1 which shows snapshot growth distributions for a specific time. Thus the averages do not necessarily indicate the mixing state of the aerosol as the temporal variability increases the spread. Most of the time at the JFJ one expects to encounter non-disturbed FT conditions or PBL INF during summer. It has been shown

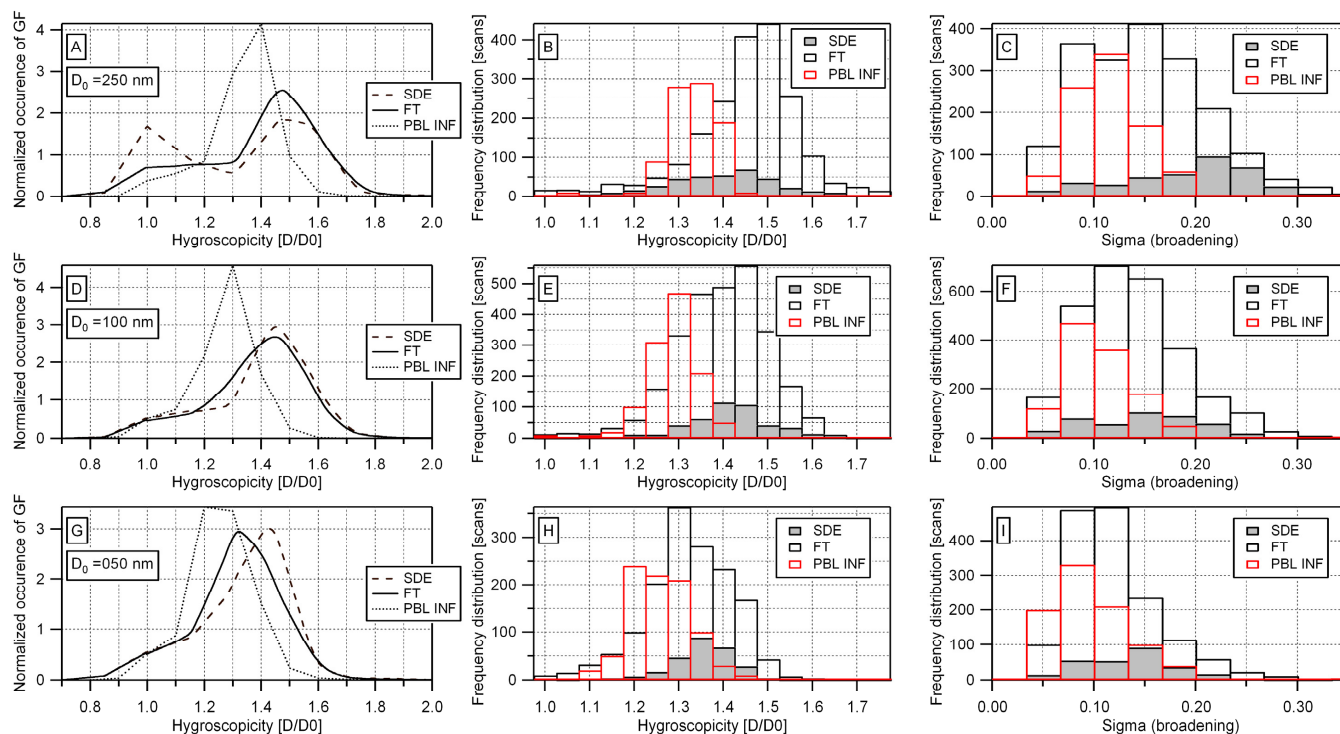


**Fig. 5.** Results for RH=85% and dry sizes  $D_0=250$ , 100, 50 nm are presented from top to bottom row. First column shows the  $GF$  distribution for SDE, FT and PBL INF conditions. Second column shows the frequency distribution of  $GF^*$ . Third column shows the frequency distribution of the spread  $\sigma$ , a measure for the broadening of the  $GF$  distribution.

in Collaud Coen et al. (2004) that SDE are present only 5% of the time (yearly average). For the FT conditions the 50 and 100 nm particles appear internally mixed, however with a small fraction of particles with a  $GF$  between 1.0–1.2, which is not easily resolved with the inversion considering the instrument limits and the low mass loading. For the 50 nm particles this shoulder at low  $GF$ s is less pronounced, but this is to some extent a consequence of the smaller hygroscopicity of the main mode, which is slightly overlapping with this shoulder. Kandler and Schütz (2007) also reported  $GF$  values for March 2000 at the JFJ (measured at 90% RH at  $\sim 20^\circ\text{C}$ ), which are in agreement with the  $GF$ s shown here. Kandler and Schütz (2007) indicated a bimodal distribution for all sizes, however they do not show the relative number fractions in each mode, which, if small for the lower  $GF$  mode, would be in agreement with our data. The PBL INF measurements show a more homogeneous  $GF$  distribution, but the hygroscopicity is also lower. SDE only occurred during the two winter campaigns, and for these cases the  $D_0=250$  nm particles showed an increase of non-hygroscopic particles in a distinct mode with a  $GF$  of 1.0. The hygroscopic properties of the  $D_0=50$  and 100 nm particles do not differ between SDE/FT. Panels (B), (E), and (H) of Fig. 5 show the frequency distribution of  $GF^*$ , from which the mean and median  $GF^*$  presented in Table 3 have been calculated. Both summer and winter measurements revealed a size dependence of growth factors. This trend is stronger than just the

influence of the Kelvin effect, as can be seen from the  $k$ -values shown in Fig. 3a. Furthermore, the observed growth factors were generally smaller in summer compared to winter, which is explained by a higher organic mass fraction in summer.

Panels C, F and I of Fig. 5 show the frequency distribution of  $\sigma$  averaged for each of the relevant periods. The  $\sigma$  of individual scans can be used to distinguish between quasi-internally mixed aerosols with limited growth factor spread ( $\sigma \leq 0.1$ ) and externally or quasi-internally mixed aerosols with substantial spread ( $\sigma \geq 0.15$ ). The frequency distribution of  $\sigma$  thus indicates the fraction of time of each period that a certain mixing state ( $\sigma$ ) is encountered. The most frequent spread observed in summer is  $\sigma \sim 0.125$  which is internally mixed, whereas larger spread is seen in winter FT conditions. This can be attributed to a larger separation of the main growth mode from the minor fraction of particles with growth factors  $< 1.2$ . For the same reason the spread also increases with particle size in winter with  $\sigma \sim 0.1$ , 0.125 and 0.15 for  $D_0=50$ , 100 and 250 nm particles, respectively. This indicates that even under FT conditions observed during winter the aerosol contains a fraction of particles which appear to remain less processed and thus less hygroscopic also at a remote location. The mineral dust during SDE mostly influences the larger particles with  $D_0=250$  nm, as already exemplified in Figs. 3 and 5A. Here it has to be stressed that different scenarios can end up with a bimodal shape of the mean

*GF* distributions as shown in Fig. 5A. Either the *GF* distribution is always bimodal with similar number fractions of particles in both modes, or only monomodal but the *GF* distribution are observed with the mode centered at  $GF \sim 1.0$  or  $GF \sim 1.45$  during 50% of the time each. Frequent occurrence of  $\sigma \geq 0.2$  and  $GF^* = 1.3\text{--}1.5$  for  $D_0 = 250$  nm during SDE indicates that the former alternative with simultaneous presence of non-hygroscopic mineral dust and more hygroscopic background particles, both in comparable number fractions, dominates. No clear influence of SDE on  $\sigma$  and  $GF^*$  is seen at 50 and 100 nm confirming the finding from Panels (D) and (G).

The frequency distributions of the  $GF^*$  and  $\sigma$  can be used to simulate internally or quasi-internally mixed hygroscopic behavior of particles in different air masses encountered at the JFJ. Additionally to the frequency distributions it has to be known whether  $GF^*$  and  $\sigma$  are dependent on each other. We explored the relationship between the two distributions, but no dependence between  $GF^*$  and  $\sigma$  was found. This is different from results found by Aklilu and Mozurkewich (2004) in the Lower Fraser Valley, British Columbia, who reported a horseshoe-shaped relationship with maximum  $\sigma$  values at intermediate *GF*.

#### 4 Conclusions

A statistical analysis of measurements from four field campaigns of about one month each at the high alpine site Jungfraujoch is presented. During the winter season when the station was in the undisturbed free troposphere, the average *GF* measured with an HTDMA was  $1.40 \pm 0.11$  at 85% RH for  $D_0 = 100$  nm particles. During the summer season, due to higher SOA formation, the *GF* was  $1.29 \pm 0.08$  at 85% RH. During mineral dust events *GF* distributions were partly bimodal for  $D_0 = 250$  nm particles. The frequency distributions of the width of the retrieved growth factor (internally/externally mixed) distributions are presented, which can be used for comparison with simulations of the hygroscopic behavior of the aerosol encountered at the JFJ.

The apparent ensemble mean *GF* of the organics encountered at the Jungfraujoch was estimated to be  $GF_{\text{org}} \approx 1.20$  at  $a_w = 0.85$  based on inverse ZSR modelling. This value is at the upper end of previous laboratory and field data though still in agreement with the highly aged and oxidized nature of the Jungfraujoch aerosol.

**Acknowledgements.** This work was supported by the Swiss National Science Foundation Switzerland (grant no 200021-100280), MeteoSwiss in the framework of the Global Atmosphere Watch Program as well as the EC projects ACCENT and EUSAAR. The UMan measurements were supported by the UK Natural Environment Research Council. We thank the International Foundation High Altitude Research Stations Jungfraujoch and Gornergrat (HFSJG), who made it possible for us to carry out our experiments at the High Altitude Research Station at Jungfraujoch, and also the caretakers at the station.

Edited by: W. Conant

#### References

- Aklilu, Y. A. and Mozurkewich, M.: Determination of external and internal mixing of organic and inorganic aerosol components from hygroscopic properties of submicrometer particles during a field study in the Lower Fraser Valley, *Aerosol Sci. Technol.*, 38, 140–154, 2004.
- Aklilu, Y., Mozurkewich, M., Prenni, A. J., Kreidenweis, S. M., Alfarra, M. R., Allan, J. D., Anlauf, K., Brook, J., Leitch, W. R., Sharma, S., Boudries, H., and Worsnop, D. R.: Hygroscopicity of particles at two rural, urban influenced sites during Pacific 2001: Comparison with estimates of water uptake from particle composition, *Atmos. Environ.*, 40, 2650–2661, 2006.
- Alfarra, M. R.: Insights into atmospheric organic aerosols using an aerosol mass spectrometer, PhD thesis, The University of Manchester, 7, 162–201, 2004.
- Alfarra, M. R., Paulsen, D., Gysel, M., Garforth, A. A., Dommen, J., Prevot, A. S. H., Worsnop, D. R., Baltensperger, U., and Coe, H.: A mass spectrometric study of secondary organic aerosols formed from the photooxidation of anthropogenic and biogenic precursors in a reaction chamber, *Atmos. Chem. Phys.*, 6, 5279–5293, 2006, <http://www.atmos-chem-phys.net/6/5279/2006/>.
- Allan, J. D., Jimenez, J. L., Williams, P. I., Alfarra, M. R., Bower, K. N., Jayne, J. T., Coe, H., and Worsnop, D. R.: Quantitative sampling using an Aerodyne aerosol mass spectrometer: 1. Techniques of data interpretation and error analysis, *J. Geophys. Res.*, 108, 4090, doi:10.1029/2002JD002358, 2003.
- Allan, J. D., Delia, A. E., Coe, H., Bower, K. N., Alfarra, M. R., Jimenez, J. L., Middlebrook, A. M., Drewnick, F., Onasch, T. B., Canagaratna, M. R., Jayne, J. T., and Worsnop, D. R.: A generalised method for the extraction of chemically resolved mass spectra from Aerodyne aerosol mass spectrometer data, *J. Aerosol Sci.*, 35(7), 909–922, 2004.
- Allan, J. D., Baumgardner, D., Raga, G. B., Mayol-Bracero, O. L., Morales-García, F., García-García, F., Montero-Martínez, G., Borrmann, S., Schneider, J., Mertes, S., Walter, S., Gysel, M., Dusek, U., Frank, G. P., and Krämer, M.: Clouds and aerosols in Puerto Rico – a new evaluation, *Atmos. Chem. Phys.*, 8, 1293–1309, 2008, <http://www.atmos-chem-phys.net/8/1293/2008/>.
- Baltensperger, U., Gäggeler, H. W., Jost, D. T., Lugauer, M., Schwikowski, M., Weingartner, E., and Seibert, P.: Aerosol climatology at the high-alpine site Jungfraujoch, Switzerland, *J. Geophys. Res.*, 102, 19 707–19 715, 1997.
- Baltensperger, U., Schwikowski, M., Jost, D. T., Nyeki, S., Gäggeler, H. W., and Poulida, O.: Scavenging of atmospheric constituents in mixed phase clouds at the high-alpine site

- Jungfraujoch part I: Basic concept and aerosol scavenging by clouds, *Atmos. Environ.*, 32, 3975–3983, 1998.
- Baltensperger, U., Kalberer, M., Dommen, J., Paulsen, D., Alfarra, M. R., Coe, H., Fisseha, R., Gascho, A., Gysel, M., Nyeki, S., Sax, M., Steinbacher, M., Prevot, A. S. H., Sjögren, S., Weingartner, E., and Zenobi, R.: Secondary organic aerosols from anthropogenic and biogenic precursors, *Faraday Discuss.*, 130, 265–278, 2005.
- Buzorius, G., Zelenyuk, A., Brechtel, F., and Imre, D.: Simultaneous determination of individual ambient particle size, hygroscopicity and composition. *Geophys. Res. Lett.*, 29, 1974, doi:10.1029/2001GL014221, 2002.
- Canagaratna, M. R., Jayne, J. T., Jimenez, J. L., Allan, J. D., Alfarra, M. R., Zhang, Q., Onasch, T. B., Drewnick, F., Coe, H., Middlebrook, A., Delia, A., Williams, L. R., Trimborn, A. M., Northway, M. J., DeCarlo, P. F., Kolb, C. E., Davidovits, P., and Worsnop, D. R.: Chemical and microphysical characterization of ambient aerosols with the Aerodyne aerosol mass spectrometer, *Mass Spectrom. Rev.*, 26, 185–222, 2007.
- Carrico, C. M., Kreidenweis, S. M., Malm, W. C., Day, D. E., Lee, T., Carrillo, J., McMeeking, G. R., and Collett Jr., J. L.: Hygroscopic growth behavior of a carbon-dominated aerosol in Yosemite National Park, *Atmos. Environ.*, 39, 1393–1404, 2005.
- Collaud Coen, M., Weingartner, E., Schaub, D., Hueglin, C., Corrigan, C., Henning, S., Schwikowski, M., and Baltensperger, U.: Saharan dust events at the Jungfraujoch: detection by wavelength dependence of the single scattering albedo and first climatology analysis, *Atmos. Chem. Phys.*, 4, 2465–2480, 2004, <http://www.atmos-chem-phys.net/4/2465/2004/>.
- Collaud Coen, M., Weingartner, E., Nyeki, S., Cozic, J., Henning, S., Verheggen, B., Gehrig, R., and Baltensperger, U.: Long-term trend analysis of aerosol variables at the high-alpine site Jungfraujoch, *J. Geophys. Res.*, 112, D13213, doi:10.1029/2006JD007995, 2007.
- Cozic, J., Verheggen, B., Mertes, S., Connolly, P., Bower, K., Petzold, A., Baltensperger, U., and Weingartner, E.: Scavenging of black carbon in mixed phase clouds at the high alpine site Jungfraujoch, *Atmos. Chem. Phys.*, 7, 1797–1807, 2007, <http://www.atmos-chem-phys.net/7/1797/2007/>.
- Cozic, J., Verheggen, B., Weingartner, E., Crosier, J., Bower, K. N., Flynn, M., Coe, H., Henning, S., Steinbacher, M., Henne, S., Collaud Coen, M., Petzold, A., and Baltensperger, U.: Chemical composition of free tropospheric aerosol for PM1 and coarse mode at the high alpine site Jungfraujoch, *Atmos. Chem. Phys.*, 8, 407–423, 2008a, <http://www.atmos-chem-phys.net/8/407/2008/>.
- Cozic, J., Mertes, S., Verheggen, B., Cziczo, D. J., Gallavardin, S. J., Walter, S., Baltensperger, U., and Weingartner, E.: Black carbon enrichment in atmospheric ice particle residuals observed in lower tropospheric mixed phase clouds, *J. Geophys. Res.*, 113, D15209, doi:10.1029/2007JD009266, 2008b.
- Cubison, M. J., Coe, H., and Gysel, M.: A modified hygroscopic tandem DMA and a data retrieval method based on optimal estimation, *J. Aerosol Sci.*, 36, 846–865, 2005.
- Dick, W. D., Saxena, P., and McMurry, P. H.: Estimation of water uptake by organic compounds in submicron aerosols measured during the Southeastern Aerosol and Visibility Study, *J. Geophys. Res.*, 105, 1471–1479, 2000.
- Dinar, E., Mentel, T. F., and Rudich, Y.: The density of humic acids and humic like substances (HULIS) from fresh and aged wood burning and pollution aerosol particles, *Atmos. Chem. Phys.*, 6, 5213–5224, 2006, <http://www.atmos-chem-phys.net/6/5213/2006/>.
- Duplissy, J., Gysel, M., Alfarra, M. R., Dommen, J., Metzger, A., Prevot, A. S. H., Weingartner, E., Laaksonen, A., Raatikainen, T., Good, N., Turner, S. F., McFiggans, G., and Baltensperger, U.: The cloud forming potential of secondary organic aerosol under near atmospheric conditions, *Geophys. Res. Lett.*, 35, L03818, doi:10.1029/2007GL031075, 2008.
- Gysel, M., Weingartner, E., and Baltensperger, U.: Hygroscopicity of aerosol particles at low temperatures. 2. Theoretical and experimental hygroscopic properties of laboratory generated aerosols, *Environ. Sci. Technol.*, 36, 63–68, 2002.
- Gysel, M., Weingartner, E., Nyeki, S., Paulsen, D., Baltensperger, U., Galambos, I., and Kiss, G.: Hygroscopic properties of water-soluble matter and humic-like organics in atmospheric fine aerosol, *Atmos. Chem. Phys.*, 4, 35–50, 2004, <http://www.atmos-chem-phys.net/4/35/2004/>.
- Gysel, M., Crosier, J., Topping, D. O., Whitehead, J. D., Bower, K. N., Cubison, M. J., Williams, P. I., Flynn, M. J., McFiggans, G. B., and Coe, H.: Closure study between chemical composition and hygroscopic growth of aerosol particles during TORCH2, *Atmos. Chem. Phys.*, 7, 6131–6144, 2007, <http://www.atmos-chem-phys.net/7/6131/2007/>.
- Henning, S., Weingartner, E., Schmidt, S., Wendisch, M., Gäggeler, H. W., and Baltensperger, U.: Size-dependent aerosol activation at the high-alpine site Jungfraujoch (3580 m a.s.l.), *Tellus*, 54B, 82–95, 2002.
- Henning, S., Weingartner, E., Schwikowski, M., Gäggeler, H. W., Gehrig, R., Hinz, K. P., Trimborn, A., Spengler, B., and Baltensperger, U.: Seasonal variation of water-soluble ions of the aerosol at the high-alpine site Jungfraujoch (3580 m a.s.l.), *J. Geophys. Res.*, 108, 4030, doi:10.1029/2002JD002439, 2003.
- Jayne, J. T., Leard, D. C., Zhang, X. F., Davidovits, P., Smith, K. A., Kolb, C. E., and Worsnop, D. R.: Development of an aerosol mass spectrometer for size and composition analysis of submicron particles, *Aerosol Sci. Technol.*, 33, 49–70, 2000.
- Jimenez, J. L., Jayne, J. T., Shi, Q., Kolb, C. E., Worsnop, D. R., Yourshaw, I., Seinfeld, J. H., Flagan, R. C., Zhang, X. F., Smith, K. A., Morris, J. W., and Davidovits, P.: Ambient aerosol sampling using the Aerodyne Aerosol Mass Spectrometer, *J. Geophys. Res.*, 108, 8425, doi:10.1029/2001JD001213, 2003.
- Kanakidou, M., Seinfeld, J. H., Pandis, S. N., Barnes, I., Dentener, F. J., Facchini, M. C., Van Dingenen, R., Ervens, B., Nenes, A., Nielsen, C. J., Swietlicki, E., Putaud, J. P., Balkanski, Y., Fuzzi, S., Horth, J., Moortgat, G. K., Winterhalter, R., Myhre, C. E. L., Tsigaridis, K., Vignati, E., Stephanou, E. G., and Wilson, J.: Organic aerosol and global climate modelling: a review, *Atmos. Chem. Phys.*, 5, 1053–1123, 2005, <http://www.atmos-chem-phys.net/5/1053/2005/>.
- Kandler, K. and Schütz, L.: Climatology of the average water-soluble volume fraction of atmospheric aerosol, *Atmos. Res.*, 83, 77–92, 2007.
- Kreidenweis, S. M., Koehler, K., DeMott, P. J., Prenni, A. J., Carrico, C., and Ervens, B.: Water activity and activation diameters from hygroscopicity data - Part I: Theory and application to inorganic salts, *Atmos. Chem. Phys.*, 5, 1357–1370, 2005, <http://www.atmos-chem-phys.net/5/1357/2005/>.

- Krivacsy, Z., Gelencser, A., Kiss, G., Meszaros, E., Molnar, A., Hoffer, A., Meszaros, T., Sarvari, Z., Temesi, D., Varga, B., Baltensperger, U., Nyeki, S., and Weingartner, E.: Study on the chemical character of water soluble organic compounds in fine atmospheric aerosol at the Jungfrauoch, *J. Atmos. Chem.*, 39, 235–259, 2001.
- Liu, B. Y. H., Pui, D. Y. H., Whitby, K. T., Kittelson, D. B., Kousaka, Y., and McKenzie, R. L.: The Aerosol Mobility Chromatograph: a new detector for sulfuric acid aerosols, *Atmos. Environ.*, 12, 99–104, 1978.
- Lugauer, M., Baltensperger, U., Furger, M., Gäggeler, H. W., Jost, D. T., Nyeki, S., and Schwikowski, M.: Influences of vertical transport and scavenging on aerosol particle surface area and radon decay product concentrations at the Jungfrauoch (3454 m a.s.l.), *J. Geophys. Res.*, 105, 19 869–19 879, 2000.
- Marcolli, C., Luo, B. P., and Peter, T.: Mixing of the organic aerosol fractions: Liquids as the thermodynamically stable phases, *J. Phys. Chem.*, 108, 2216–2224, 2004.
- Marcolli, C. and Krieger, U. K.: Phase changes during hygroscopic cycles of mixed organic/inorganic model systems of tropospheric aerosols, *J. Phys. Chem.*, 110, 1881–1893, 2006.
- McFiggans, G., Artaxo, P., Baltensperger, U., Coe, H., Facchini, M. C., Feingold, G., Fuzzi, S., Gysel, M., Laaksonen, A., Lohmann, U., Mentel, T. F., Murphy, D. M., O'Dowd, C. D., Snider, J. R., and Weingartner, E.: The effect of physical and chemical aerosol properties on warm cloud droplet activation, *Atmos. Chem. Phys.*, 6, 2593–2649, 2006, <http://www.atmos-chem-phys.net/6/2593/2006/>.
- Mertes, S., Verheggen, B., Walter, S., Ebert, M., Connolly, P., Weingartner, E., Schneider, J., Bower, K. N., Inerle-Hof, M., Cozic, J., Baltensperger, U., and Heintzenberg, J.: Counterflow virtual impactor based collection of small ice particles in mixed-phase clouds for the physico-chemical characterisation of tropospheric ice nuclei: sampler description and first case study, *Aerosol Sci. Technol.*, 41, 848–864, 2007.
- Nyeki, S., Li, F., Weingartner, E., Streit, N., Colbeck, I., Gäggeler, H. W., and Baltensperger, U.: The background aerosol size distribution in the free troposphere: An analysis of the annual cycle at a high-alpine site, *J. Geophys. Res.*, 103, 31 749–31 761, 1998.
- Nyeki, S., Kalberer, M., Colbeck, I., De Wekker, S., Furger, M., Gäggeler, H. W., Kossmann, M., Lugauer, M., Steyn, D., Weingartner, E., Wirth, M., and Baltensperger, U.: Convective boundary layer evolution to 4 km a.s.l. over high-alpine terrain: Airborne lidar observations in the Alps, *Geophys. Res. Lett.*, 27, 689–692, 2000.
- Putaud, J. P., Raes, F., Van Dingenen, R., Brüggemann, E., Facchini, M. C., Decesari, S., Fuzzi, S., Gehrig, R., Hüglin, C., Laj, P., Lorbeer, G., Maenhaut, W., Mihalopoulos, N., Müller, K., Querol, X., Rodriguez, S., Schneider, J., Spindler, G., ten Brink, H., Tørseth, K., and Wiedensohler, A.: European aerosol phenomenology-2: chemical characteristics of particulate matter at kerbside, urban, rural and background sites in Europe, *Atmos. Environ.*, 38, 2579–2595, 2004.
- Rader, D. J. and McMurry, P. H.: Application of the tandem differential mobility analyzer to studies of droplet growth or evaporation, *J. Aerosol Sci.*, 17, 771–787, 1986.
- Randall, D. A., Wood, R. A., Bony, S., Colman, R., Fichet, T., Fyfe, J., Kattsov, V., Pitman, A., Shukla, J., Srinivasan, J., Stouffer, R. J., Sumi, A., and Taylor, K. E.: Contribution of Working Group I to the Fourth Assessment Report of the Intergovernmental Panel on Climate Change – Climate Models and their Evaluation, Cambridge University Press, Cambridge, United Kingdom and New York, 589–662, 2007.
- Sjogren, S., Gysel, M., Weingartner, E., Baltensperger, U., Cubison, M. J., Coe, H., Zardini, A. A., Marcolli, C., Krieger, U. K., and Peter, T.: Hygroscopic growth and water uptake kinetics of two-phase aerosol particles consisting of ammonium sulfate, adipic and humic acid mixtures, *J. Aerosol Sci.*, 38, 157–171, 2007.
- Solomon, S., Qin, D., Manning, M., Alley, R. B., Bernsten, T., Bindoff, N. L., Chen, Z., Chidthaisong, A., Gregory, J. M., Hegerl, G. C., Heimann, M., Hewitson, B., Hoskins, B. J., Joos, F., Jouzel, J., Kattsov, V., Lohmann, U., Matsuno, T., Molina, M., Nicholls, N., Overpeck, J., Raga, G., Ramaswamy, V., Ren, J., Rusticucci, M., Somerville, R., Stocker, T. F., Whetton, P., Wood, R. A., and Wratt, D.: Contribution of Working Group I to the Fourth Assessment Report of the Intergovernmental Panel on Climate Change – Technical Summary, Cambridge University Press, Cambridge, UK and NY, 19–92, 2007.
- Stokes, R. H. and Robinson, R. A.: Interactions in aqueous non-electrolyte solutions. I. Solute-solvent equilibria, *J. Phys. Chem.*, 70, 2126–2130, 1966.
- Stolzenburg, M. R. and McMurry, P. H.: TDMAFIT user's manual, University of Minnesota, Department of Mechanical Engineering, Particle Technology Laboratory, 1–80, Minneapolis, 1988.
- Swietlicki, E., Zhou, J. C., Covert, D. S., Hämeri, K., Busch, B., Vakeva, M., Dusek, U., Berg, O. H., Wiedensohler, A., Aalto, P., Makela, J., Martinsson, B. G., Papaspiropoulos, G., Mentes, B., Frank, G., and Stratmann, F.: Hygroscopic properties of aerosol particles in the northeastern Atlantic during ACE-2, *Tellus*, 52, 201–227, 2000.
- Swietlicki, E., Hansson, H.-C., Hämeri, K., Svenningsson, B., Massling, A., McFiggans, G., McMurry, P. H., Petäjä, T., Tunved, P., Gysel, M., Topping, D., Weingartner, E., Baltensperger, U., Rissler, J., Wiedensohler, A., and Kulmala, M.: Hygroscopic properties of sub-micrometer atmospheric aerosol particles measured with H-TDMA instruments in various environments – a review, *Tellus B*, 60, 432–469, 2008.
- Topping, D. O., McFiggans, G. B., and Coe, H.: A curved multicomponent aerosol hygroscopicity model framework: Part 2 – Including organic compounds, *Atmos. Chem. Phys.*, 5, 1223–1242, 2005a, <http://www.atmos-chem-phys.net/5/1223/2005/>.
- Topping, D. O., McFiggans, G. B., and Coe, H.: A curved multicomponent aerosol hygroscopicity model framework: Part 1 – Inorganic compounds, *Atmos. Chem. Phys.*, 5, 1205–1222, 2005b, <http://www.atmos-chem-phys.net/5/1205/2005/>.
- Varutbangkul, V., Brechtel, F. J., Bahreini, R., Ng, N. L., Keywood, M. D., Kroll, J. H., Flagan, R. C., Seinfeld, J. H., Lee, A., and Goldstein, A. H.: Hygroscopicity of secondary organic aerosols formed by oxidation of cycloalkenes, monoterpenes, sesquiterpenes, and related compounds, *Atmos. Chem. Phys.*, 6, 2367–2388, 2006, <http://www.atmos-chem-phys.net/6/2367/2006/>.
- Verheggen, B., Cozic, J., Weingartner, E., Bower, K., Mertes, S., Connolly, P., Flynn, M., Gallagher, M., Choulaton, T., and Baltensperger, U.: Aerosol partitioning between the interstitial and the condensed phase in mixed-phase clouds, *J. Geophys. Res.*, 112, D23202, doi:10.1029/2007JD008714, 2007.
- Vlasenko, A., Sjogren, S., Weingartner, E., Stemmler, K., Gäggeler, H. W., and Ammann, M.: Effect of humidity on nitric acid uptake

- to mineral dust aerosol particles, *Atmos. Chem. Phys.*, 6, 2147–2160, 2006, <http://www.atmos-chem-phys.net/6/2147/2006/>.
- Weingartner, E., Nyeki, S., and Baltensperger, U.: Seasonal and diurnal variation of aerosol size distributions ( $10 < D < 750$  nm) at a high-alpine site (Jungfraujoch 3580 m a.s.l.), *J. Geophys. Res.*, 104, 26 809–26 820, 1999.
- Weingartner, E., Gysel, M., and Baltensperger, U.: Hygroscopicity of aerosol particles at low temperatures. 1. New low-temperature H-TDMA instrument: Setup and first applications, *Environ. Sci. Technol.*, 36, 55–62, 2002.
- Weingartner, E., Saathoff, H., Schnaiter, M., Streit, N., Bitnar, B., and Baltensperger, U.: Absorption of light by soot particles: determination of the absorption coefficient by means of aethalometers, *J. Aerosol Sci.*, 34, 1445–1463, 2003.
- Zelenyuk, A., Cai, Y., and Imre, D.: From agglomerates of spheres to irregularly shaped particles: Determination of dynamic shape factors from measurements of mobility and vacuum aerodynamic diameters, *Aerosol Sci. Technol.*, 40, 197–217, 2006.
- Zhang, Q., Alfarra, M. R., Worsnop, D. R., Allan, J. D., Coe, H., Canagaratna, M. R., and Jimenez, J. L.: Deconvolution and quantification of hydrocarbon-like and oxygenated organic aerosols based on aerosol mass spectrometry, *Environ. Sci. Technol.*, 39, 4938–4952, 2005.
- Zhang, Q., Jimenez, J. L., Canagaratna, M. R., Allan, J. D., Coe, H., Ulbrich, I., Alfarra, M. R., Takami, A., Middlebrook, A. M., Sun, Y. L., Dzepina, K., Dunlea, E., Docherty, K., DeCarlo, P. F., Salcedo, D., Onasch, T., Jayne, J. T., Miyoshi, T., Shimojo, A., Hatakeyama, S., Takegawa, N., Kondo, Y., Schneider, J., Drewnick, F., Borrmann, S., Weimer, S., Demerjian, K., Williams, P., Bower, K., Bahreini, R., Cottrell, L., Griffin, R. J., Rautiainen, J., Sun, J. Y., Zhang, Y. M., and Worsnop, D. R.: Ubiquity and dominance of oxygenated species in organic aerosols in anthropogenically-influenced Northern Hemisphere midlatitudes, *Geophys. Res. Lett.*, 34, L13801, doi:10.1029/2007GL029979, 2007.